Applied Physics Letters

High coherence superconducting microwave cavities with indium bump bonding

Cite as: Appl. Phys. Lett. **116**, 154002 (2020); https://doi.org/10.1063/5.0003907
Submitted: 06 February 2020 • Accepted: 26 March 2020 • Published Online: 15 April 2020

Chan U Lei, Lev Krayzman, Suhas Ganjam, et al.

Applied Physics Letters ARTICLE scitation.org/journal/apl

High coherence superconducting microwave cavities with indium bump bonding

Cite as: Appl. Phys. Lett. **116**, 154002 (2020); doi: 10.1063/5.0003907
Submitted: 6 February 2020 · Accepted: 26 March 2020 ·
Published Online: 15 April 2020

Chan U Lei,[1,2,a)] Lev Krayzman,[1,2,b)] Suhas Ganjam,[1,2] Luigi Frunzio,[1,2] and Robert J. Schoelkopf[1,2,c)]

AFFILIATIONS

[1]Department of Applied Physics, Yale University, New Haven, Connecticut 06511, USA
[2]Yale Quantum Institute, Yale University, New Haven, Connecticut 06520, USA

[a)]Author to whom correspondence should be addressed: chanu.lei@yale.edu
[b)]Electronic mail: lev.krayzman@yale.edu
[c)]Electronic mail: robert.schoelkopf@yale.edu

ABSTRACT

Low-loss cavities are important in building high-coherence superconducting quantum computers. Generating high-quality joints between parts is crucial for the realization of a scalable quantum computer using the circuit quantum electrodynamics (cQED) framework. In this paper, we adapt the technique of indium bump bonding to cQED to realize high-quality superconducting microwave joints between chips. We use this technique to fabricate compact superconducting cavities in the multilayer microwave integrated quantum circuit (MMIQC) architecture and achieve single photon quality factors over 300×10^6 or single-photon lifetimes approaching 5 ms. To quantify the performance of the resulting seam, we fabricate microwave stripline resonators in multiple sections connected by different numbers of bonds, resulting in a wide range of seam admittances. The measured quality factors combined with the designed seam admittances allow us to bound the conductance of the seam at $g_{\text{seam}} \geq 2 \times 10^{10}/(\Omega\,\text{m})$. Such a conductance should enable the construction of micromachined superconducting cavities with a quality factor of at least a billion. These results demonstrate the capability to construct very high-quality microwave structures within the MMIQC architecture.

Circuit quantum electrodynamics (cQED) is one of the most promising platforms for quantum computation. Coherence times have been dramatically improved in the past decade.[1] Additionally, circuits with dozens of qubits have been realized and used to demonstrate many interesting results, such as molecular simulations,[2–4] condensed matter simulations,[5] and proof-of-principle quantum supremacy calculations.[6] However, further scaling up the number of circuit components while maintaining or even improving their coherence is very challenging.

In the past several years, techniques from the MEMS industry have been applied to the cQED framework to construct multilayer microwave integrated quantum circuits (MMIQCs).[7] Tremendous progress has been achieved in 3D integration of quantum circuit elements while maintaining their coherence.[8–11] Micromachined superconducting cavities can be highly useful in the MMIQC architecture. Such structures can serve as long-lived quantum memories or as enclosures to suppress radiation loss to the environment and crosstalk between quantum circuit elements. A crucial requirement for constructing high-quality micromachined superconducting cavities is the fabrication of high-quality microwave joints between layers of the MMIQC.[10] The loss associated with joints significantly limits the choice of geometries, materials, and fabrication processes of the superconducting cavities, as well as the layout of quantum circuits. To maintain the performance of superconducting cavities without sacrificing design flexibility, a qubit-compatible method to create high quality joints between parts is critically important.

In the particle accelerator community, a lot of effort has been put toward improving the joint quality in superconducting RF cavities. Methods such as diffusion-bonding[12] and electron beam welding[13] have been used to create high-quality joints. Recently, niobium cavities with the quality factor higher than 10^{10} have been demonstrated at single-photon powers.[14] Although these methods create high-quality joints between metal parts, their application to joining on-chip superconducting circuits has not been demonstrated. Therefore, integrating qubits into such cavities would require manual assembly with current technology. A better candidate for creating ultra-low loss joints for superconducting quantum circuits is indium bump bonding. It is an established method that has been used in the field of cryogenic

detectors[15] and has several properties that make it suitable for this application. Indium cold-welds to itself and is not brittle at cryogenic temperatures,[16] allowing for room-temperature bonding, which remains robust even with thermal cycling to milli-Kelvin temperatures. Additionally, it superconducts at 3.4 K and can thus form low-loss bonds. Finally, it is compatible with standard lithographic techniques, enabling the adaptation of the existing approaches for scaling up quantum circuits. Recently, indium bonding has been used for chip hybridization and interconnections.[8,17–19]

In this work, we adapt indium bump bonding to the cQED architecture. Using this technique, we create superconducting joints with very low loss at microwave frequencies. We quantify the loss of the resulting joint by fabricating bump-bonded indium stripline resonators and measuring their internal quality factors. We then apply this indium bump-bonding technique to realize high-quality micromachined cavities and show devices with a low-power quality factor of over 300×10^6.

Building superconducting cavities requires joining together at least two different parts. However, the seam at the joint may limit the coherence of a cavity resonator. In an ideal joint, the contact surfaces participating in the seam would be identical to the bulk material that comprises the remainder of the cavity; there would be no extra loss associated with the seam. In a realistic joint, imperfections such as lattice defects, metal oxides, or organic residue on the surfaces can reduce the electrical conductivity across the seam and degrade the quality of the resonator. The loss of the seam can be quantified with the following phenomenological model from Ref. 10:

$$\frac{1}{Q_{\text{seam}}} = \frac{1}{g_{\text{seam}}} \times \frac{\int_{\text{seam}} |\vec{J}_s \times \hat{l}|^2 dl}{\omega \int_{\text{tot}} \mu |\vec{H}|^2 dV} \equiv \frac{1}{g_{\text{seam}}} \times y_{\text{seam}}, \tag{1}$$

where $\hat{l}$ is a unit vector along the seam and the integral in the denominator is taken over the entire volume of the mode (see Fig. S1 in the supplementary material). The conductance per unit length g_{seam} is an empirical value, and the admittance per unit length y_{seam} is a geometric factor that can be calculated analytically or numerically.

Previous studies[10] have shown that seam loss can be dominant in a cavity, depending on the cavity geometry and location as well as quality of the seam, as shown in Fig. 1(c). Series A (black circles, data from Brecht *et al.*[10]) represents the TE110 modes of a set of rectangular cavity resonators machined out of bulk 6061 aluminum. Each device is nominally identical, except for the location of its seam. The different seam positions result in different values of y_{seam}, with higher y_{seam} corresponding to lower Q. The internal quality factors of these devices lie on a diagonal line corresponding to a $g_{\text{seam}} \approx 10^3/(\Omega\,\text{m})$.

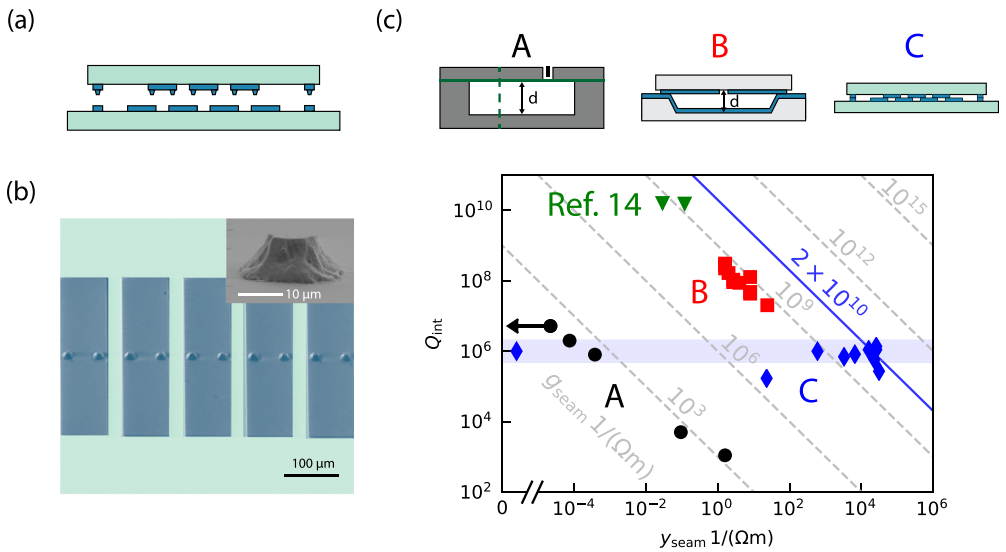

FIG. 1. (a) Schematic of the bump-bonded stripline resonator. The two chips are depicted separately, with sapphire in teal and indium in blue. The multi-section stripline is visible, with bumps on the daughter chip making the connections. Additionally, mechanical support bumps can be seen on the edges of the stripline. (b) False-colored optical micrograph of the daughter chip, with the interrupted stripline together with the bumps visible. The inset shows an SEM image of a bump. (c) Plot of measured internal Q vs simulated y_{seam} for four series of devices. Dashed diagonal lines are lines of constant g_{seam}. Series A (black circles) represents the TE101 modes of traditionally machined aluminum 6061 cavities with seams placed at varying locations. The green lines in the accompanying diagram show the locations of the seams: either along the dashed line (with varying horizontal positions) or along the solid line (with varying depths d). The arrow on the plot indicates that the device has an y_{seam} value of nominally 0 although machining imprecision can give it a non-zero y_{seam}, indicated by the position of the circle. Series B (red squares) represents micromachined cavities of differing depths. Although the points seem to lie along a line of constant g_{seam}, we note that several other loss mechanisms (metal–air interface, conductor loss) scale with the depth in the same way as y_{seam}, meaning that the cavity could be limited by any or several of these mechanisms. Series C (blue diamonds) represents the bump-bonded stripline resonators, with varying numbers of bumps. One device has an y_{seam} value of precisely 0 (indicated by a break in the x-axis), as it is a control device with the entire stripline on one chip. We generally observe a device-to-device variation of around a factor of two in the Q values of our stripline resonators, which is represented here as a blue band around the control device. If the striplines were limited by seam loss, we would expect a consistent deviation from this band. The blue line of $g_{\text{seam}} = 2 \times 10^{10}/(\Omega\,\text{m})$ is a lower bound on the seam conductance that is representative of the several devices with very large seam admittance. Finally, the green triangles represent the TM010 mode of niobium TESLA cavities,[14] with published Q_{int} values and y_{seam} that we estimated by simulated the mode structure for the published dimensions.

Since the geometries of the devices are nominally identical, the energy participation in other loss mechanisms remains fixed, while y_{seam} varies. This is consistent with their Q values being limited by seam loss. For micromachined cavities made by bonding two wafers together, the location of the joint is necessarily at the worst location for the fundamental mode, with $y_{seam} \approx 1/(\Omega\,\mathrm{m})$. In order to improve its coherence time, it is, therefore, necessary to increase g_{seam} by developing better joints.

As mentioned above, indium bump bonding is a promising method for improving the joint quality of superconducting microwave circuits. We fabricate indium bumps at the location of the joint using a variant of the standard process (see the supplementary material). Photolithography is used to lift off thermally evaporated indium, forming approximately 15 μm × 15 μm × 10 μm bumps [see the inset in Fig. 1(b)]. For the other side of the joint, we leave a uniform layer of evaporated indium. Before bonding, we treat both chips using a plasma surface treatment in order to remove oxide and passivate the surface. Finally, we bond the two chips in a commercial wafer bonder at room temperature. As the bumps are compressed, they deform, breaking through the surface oxide and forming metal-to-metal bonds, which results in a low-loss seam.

In order to characterize the quality of the resulting joint, we create indium stripline resonators in multiple sections connected by varying numbers of bump bonds [see Fig. 1(a)]. By varying the number of bumps, we can change y_{seam} of the devices. The highest y_{seam} is achieved when there are a maximum number of bumps given fabrication constraints [see Fig. 1(b)]. These devices can attain much higher y_{seam} than micromachined cavities without too much of a decrease in Q, allowing us to place a tighter lower bound on g_{seam}. A control device is also created by placing the entire stripline on one chip, which is still bonded to the second chip by the mechanical support bumps on the edge. Since such a device has no seam at all, its y_{seam} should be precisely 0.

We measure the stripline resonators in a multiplexed package in the hanger configuration at the base of a dilution refrigerator, with temperature around 15 mK.[20] Series C (blue diamonds) in Fig. 1(c) represents these devices. The control device was measured to have $Q_{int} \approx 10^6$, which is set by seam-independent losses. A shaded blue band is drawn around the control device with the width set by the normal device-to-device variation observed in stripline resonators. If the resonators are not seam-limited, we expect their Q values to consistently lie within the band. We note that this is the case for most devices except for two with lower Q, which could be caused by some imperfection in the device or the bond. This suggests that the measured Q values of the bump-bonded resonators are not limited by seam loss but rather by other mechanisms, such as dielectric or conductor losses. With these data, we place a lower bound on $g_{seam} \geq 2 \times 10^{10}/(\Omega\,\mathrm{m})$, which is representative of the distribution of several points around our highest y_{seam}. A seam with such a conductance would enable a micromachined cavity to have a Q value of 1 to 10 billion, depending on the depth.

We additionally plot two green triangles representing the TM010 mode of niobium TESLA cavities[14] for comparison. The Q_{int} values are as reported in this paper, and the y_{seam} values are obtained by simulating the mode structure of cavities with the shape and dimensions as well as the seam location set as published. It is interesting to note that lower bound on g_{seam} obtained in this manner is similar to the lower bound obtained in this work although the techniques and materials are quite different. In either case, the seam quality enables cavities with a Q_{int} value of 10^9–10^{10}. However, the particular methods used in Romaneko *et al.* require specialized processing and cannot be easily applied to creating good joints between bonded chips.[14]

The high-quality indium joint described above is, thus, a good candidate for application to enhance the lifetime of micromachined cavities, which have so far been limited by seam loss.[10] These cavities are composed of two silicon chips that are metallized with 1.2 μm of thermally evaporated indium [Fig. 2(a)]. The bottom chip contains a rectangular recess area made using a potassium hydroxide anisotropic silicon etch, resulting in a 54.7° sidewall [Fig. 2(b)]. The top chip is patterned with a coupling aperture for the measurement [inset in Fig. 2(a)]. In order to improve the seam quality, indium bump arrays are fabricated along the contact region on the top chip [dashed line on the top chip in Fig. 2(a)]. The two chips are bonded together with a commercial wafer bonder with a force of 2 kN in ambient conditions to form a micromachined cavity, which is mounted on a sample holder to be measured in a reflection configuration (see the supplementary material).

The internal loss of the micromachined cavity consists of the conductive loss of the indium, the dielectric loss of the indium oxide, and the loss from the seam formed at the contact of the two chips,

$$\frac{1}{Q_{int}} = \frac{\alpha R_s}{\omega \mu_0 \lambda_0} + p_{diel} \tan\delta + \frac{y_{seam}}{g_{seam}}. \tag{2}$$

Here, ω is the frequency of the cavity resonance, μ_0 is the vacuum permeability, and λ_0 is the penetration depth of indium. The kinetic inductance fraction α, the surface dielectric participation ratio p_{diel}, and the seam admittance per unit length y_{seam} are geometrical parameters that can be calculated analytically or numerically. The surface resistance R_s of the superconductor, the loss tangent $\tan\delta$ of the surface dielectric, and the seam conductance per unit length g_{seam} represent the intrinsic loss of each respective loss mechanism.

For the TE110 mode of the micromachined cavity, we observe that the internal quality factor increases linearly with d, as shown in Fig. 2(d). However, α, p_{diel}, and y_{seam} are all inversely proportional to the depth of the cavity d for this mode. Therefore, we cannot determine which loss mechanisms are dominant based on this set of measurements. Nevertheless, by attributing the total loss to a single loss mechanism, we can place bounds on the corresponding intrinsic loss, which gives $R_s \leq 261\,\mathrm{n}\Omega$, $\tan\delta \leq 1.2 \times 10^{-2}$, and $g_{seam} \geq 3.4 \times 10^8/(\Omega\,\mathrm{m})$. The highest internal quality factor we have achieved in this study is 3.4×10^8 with a cavity depth of $d = 1.5$ mm. The lifetimes of these cavities are independent of whether a phase-sensitive heterodyne measurement [Fig. 2(e)] or a phase-insensitive power ringdown measurement [Fig. 2(f)] is used, i.e., $T_2^* \simeq 2T_1$. Additionally, their internal quality factors depend very weakly on the average photon number $(\bar{n})$ as compared to typical coplanar waveguide (CPW) resonators. This is consistent with the fact that the mode volume of the micromachined cavities is several million times larger than that of CPW resonators (see the supplementary material). No apparent degradation in the internal quality factor has been observed after the samples have been exposed to air for over 3 months.

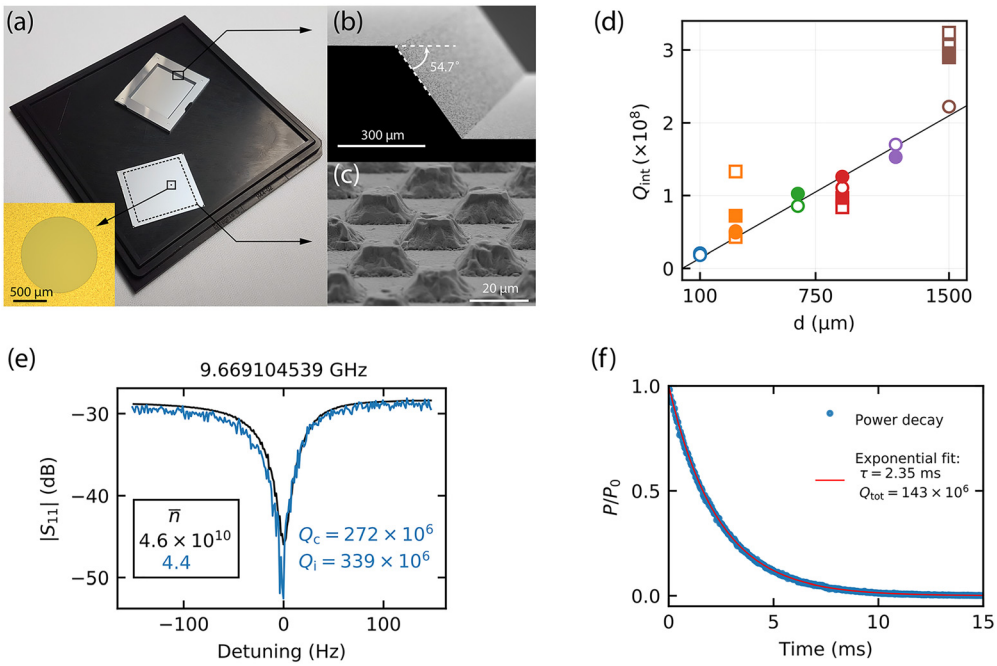

FIG. 2. (a) The top chip and the bottom chip of a micromachined cavity before bonding; the dashed line on the top chip indicates the location of the indium bumps, and the inset shows the optical micrograph of the coupling aperture on the top chip. (b) Side wall of the bottom chip. (c) Electron micrograph of the indium bumps. (d) Internal quality factor of micromachined cavities with the cavity depth equal to 100 μm (blue), 300 μm (orange), 650 μm (green), 900 μm (red), 1200 μm (purple), and 1500 μm (brown). Squares (circles) represent devices from batch 1 (2). Opened and filled symbols represent data from two cooldowns that are separated by more than 3 months. The solid line is a linear fit for devices from batch 2. (e) Transmission spectrum of a micromachined cavity with $d = 1500$ μm at 4 photons (blue) and 10^{10} photons (black). (f) Power decay measurement data (blue) and exponential fit (red).

In conclusion, we have demonstrated techniques to fabricate and characterize high-quality superconducting joints. We have used the bump-bonding technique to construct high-quality indium micromachined cavities using industry standard methods that do not require manual assembly. Using this technique, we have achieved a low-power internal quality factor of over 300×10^6 corresponding to an intrinsic T1 approaching 5 ms, which is comparable to the performance of conventionally machined cavities used for quantum memories in cQED. This result together with the ability to make low-loss joints shows that indium is a good superconductor for making high-quality quantum circuits.

Coupling a qubit to a micromachined cavity requires a slightly different design[11,21] than in other 3D circuit QED experiments using conventional machined cavities.[22] A correctly designed qubit structure on the top chip of the micromachined cavity has been shown to have adequate dipole coupling to the cavity.[11] To incorporate a qubit into the high-Q indium micromachined cavity developed in this work, the qubit is first fabricated on the top chip using e-beam lithography and double-angle aluminum evaporation. After that, the indium ground plane (which also serves as the roof of the cavity) is fabricated on the top chip using a standard photolithography process. Finally, indium bumps can be fabricated on the indium ground plane with an additional lithography step, and the indium bump-bonding technique developed in this work can be applied to improve the lifetime of a MMIQC-based quantum memory to the millisecond level.

The desire to build 3D cavities either to serve as quantum memories or to provide electromagnetic shielding highlights the fact that seam losses are very important for the 3D integration of quantum circuits. Since the scaling of superconducting circuits for quantum information processing will likely require multilayer circuits and interconnects,[8,11] the improved performance of the superconducting joints demonstrated here can be a key enabler for enhancing coherence in a wide range of devices. It also allows the realization of low-loss compact multilayer circuits including flip-chip resonators and lumped-element microwave networks. This work, thus, provides an important step toward building a more complicated MMIQC while improving its performance.

See the supplementary material for the fabrication process and the measurement setup, the calculation of the participation factors, as well as the temperature and power dependence of the micromachined cavities.

AUTHOR'S CONTRIBUTIONS

C.U.L. and L.K. contributed equally to this work.

We thank Harvey Moseley, Ari Brown, Nicholas Costen, Timothy Miller, Luke Burkhart, and Gianluigi Catelani for useful conversations; Jan Schroers and Teresa Brecht for assistance with wafer bonding; Charles Ahn, Frederick Walker, and Cristina Visani for assistance with DC measurements; Philip Reinhold and

Christopher Axline for experimental assistance; and Michael Power, Michael Rooks, Christopher Tillinghast, James Agresta, Yong Sun, Sean Rinehart, and Kelley Woods for assistance with device fabrication. This research was supported by U.S. Army Research Office Grant No. W911NF-18-1-0212. S.G. was supported by a Max Planck Research Award from the Alexander von Humboldt Foundation. Facility use was supported by the Yale University cleanroom and YINQE. R.J.S. and L.F. are founders and shareholders of Quantum Circuits Inc.

REFERENCES

[1]M. Kjaergaard, M. E. Schwartz, J. Braumüller, P. Krantz, J. I.-J. Wang, S. Gustavsson, and W. D. Oliver, "Superconducting qubits: Current state of play," Annu. Rev. Condens. Matter Phys. **11**, 369 (2020).
[2]C. S. Wang, J. C. Curtis, B. J. Lester, Y. Zhang, Y. Y. Gao, J. Freeze, V. S. Batista, P. H. Vaccaro, I. L. Chuang, L. Frunzio *et al.*, "Quantum simulation of molecular vibronic spectra on a superconducting bosonic processor," arXiv:1908.03598 (2019).
[3]A. Kandala, K. Temme, A. D. Córcoles, A. Mezzacapo, J. M. Chow, and J. M. Gambetta, "Error mitigation extends the computational reach of a noisy quantum processor," Nature **567**, 491 (2019).
[4]P. J. O'Malley, R. Babbush, I. D. Kivlichan, J. Romero, J. R. McClean, R. Barends, J. Kelly, P. Roushan, A. Tranter, N. Ding *et al.*, "Scalable quantum simulation of molecular energies," Phys. Rev. X **6**, 031007 (2016).
[5]R. Ma, B. Saxberg, C. Owens, N. Leung, Y. Lu, J. Simon, and D. I. Schuster, "A dissipatively stabilized Mott insulator of photons," Nature **566**, 51 (2019).
[6]F. Arute, K. Arya, R. Babbush, D. Bacon, J. C. Bardin, R. Barends, R. Biswas, S. Boixo, F. G. Brandao, D. A. Buell *et al.*, "Quantum supremacy using a programmable superconducting processor," Nature **574**, 505–510 (2019).
[7]T. Brecht, W. Pfaff, C. Wang, Y. Chu, L. Frunzio, M. H. Devoret, and R. J. Schoelkopf, "Multilayer microwave integrated quantum circuits for scalable quantum computing," npj Quantum Inf. **2**, 16002 (2016).
[8]D. Rosenberg, D. Kim, R. Das, D. Yost, S. Gustavsson, D. Hover, P. Krantz, A. Melville, L. Racz, G. Samach *et al.*, "3D integrated superconducting qubits," npj Quantum Inf. **3**, 42 (2017).
[9]A. Dunsworth, R. Barends, Y. Chen, Z. Chen, B. Chiaro, A. Fowler, B. Foxen, E. Jeffrey, J. Kelly, P. Klimov *et al.*, "A method for building low loss multi-layer wiring for superconducting microwave devices," Appl. Phys. Lett. **112**, 063502 (2018).
[10]T. Brecht, M. Reagor, Y. Chu, W. Pfaff, C. Wang, L. Frunzio, M. H. Devoret, and R. J. Schoelkopf, "Demonstration of superconducting micromachined cavities," Appl. Phys. Lett. **107**, 192603 (2015).
[11]T. Brecht, Y. Chu, C. Axline, W. Pfaff, J. Z. Blumoff, K. Chou, L. Krayzman, L. Frunzio, and R. J. Schoelkopf, "Micromachined integrated quantum circuit containing a superconducting qubit," Phys. Rev. Appl. **7**, 044018 (2017).
[12]S. Isagawa, "Fabrication of a superconducting niobium cavity by the diffusion-bonding method," J. Appl. Phys. **49**, 881–885 (1978).
[13]M. Allen, Z. Farkas, H. Hogg, E. Hoyt, and P. Wilson, "Superconducting niobium cavity measurements at SLAC," IEEE Trans. Nucl. Sci. **18**, 168–172 (1971).
[14]A. Romanenko, R. Pilipenko, S. Zorzetti, D. Frolov, M. Awida, S. Belomestnykh, S. Posen, and A. Grassellino, "Three-dimensional superconducting resonators at $T < 20$ mK with photon lifetimes up to $\tau = 2$ s," Phys. Rev. Appl. **13**, 034032 (2020).
[15]N. DeNigris, J. Chervenak, S. Bandler, M. Chang, N. Costen, M. Eckart, J. Ha, C. Kilbourne, and S. Smith, "Fabrication of flexible superconducting wiring with high current-carrying capacity indium interconnects," J. Low Temp. Phys. **193**, 687–694 (2018).
[16]M. Datta, T. Osaka, and J. W. Schultze, *Microelectronic Packaging* (CRC Press, 2004).
[17]B. Foxen, J. Y. Mutus, E. Lucero, R. Graff, A. Megrant, Y. Chen, C. Quintana, B. Burkett, J. Kelly, E. Jeffrey, Y. Yang, A. Yu, K. Arya, R. Barends, Z. Chen, B. Chiaro, A. Dunsworth, A. Fowler, C. Gidney, M. Giustina, T. Huang, P. Klimov, M. Neeley, C. Neill, P. Roushan, D. Sank, A. Vainsencher, J. Wenner, T. C. White, and J. M. Martinis, "Qubit compatible superconducting interconnects," Quantum Sci. Technol. **3**, 014005 (2018).
[18]W. O'Brien, M. Vahidpour, J. T. Whyland, J. Angeles, J. Marshall, D. Scarabelli, G. Crossman, K. Yadav, Y. Mohan, C. Bui *et al.*, "Superconducting caps for quantum integrated circuits," arXiv:1708.02219 (2017).
[19]C. McRae, J. Béjanin, Z. Pagel, A. Abdallah, T. McConkey, C. Earnest, J. Rinehart, and M. Mariantoni, "Thermocompression bonding technology for multilayer superconducting quantum circuits," Appl. Phys. Lett. **111**, 123501 (2017).
[20]C. Axline, M. Reagor, R. Heeres, P. Reinhold, C. Wang, K. Shain, W. Pfaff, Y. Chu, L. Frunzio, and R. J. Schoelkopf, "An architecture for integrating planar and 3D CQED devices," Appl. Phys. Lett. **109**, 042601 (2016).
[21]Z. Minev, K. Serniak, I. Pop, Z. Leghtas, K. Sliwa, M. Hatridge, L. Frunzio, R. J. Schoelkopf, and M. Devoret, "Planar multilayer circuit quantum electrodynamics," Phys. Rev. Appl. **5**, 044021 (2016).
[22]M. Reagor, W. Pfaff, C. Axline, R. W. Heeres, N. Ofek, K. Sliwa, E. Holland, C. Wang, J. Blumoff, K. Chou, M. J. Hatridge, L. Frunzio, M. H. Devoret, L. Jiang, and R. J. Schoelkopf, "Quantum memory with millisecond coherence in circuit QED," Phys. Rev. B **94**, 014506 (2016).